

## Microscopic investigation of electronic inhomogeneity induced by substitutions in a quantum critical metal CeCoIn<sub>5</sub>

H. Sakai,<sup>1,\*</sup> F. Ronning,<sup>2</sup> J.-X. Zhu,<sup>3</sup> N. Wakeham,<sup>2</sup> H. Yasuoka,<sup>2</sup> Y. Tokunaga,<sup>1</sup> S. Kambe,<sup>1</sup> E. D. Bauer,<sup>2</sup> and J. D. Thompson<sup>2</sup>

<sup>1</sup>Advanced Science Research Center, Japan Atomic Energy Agency, Tokai, Ibaraki 319-1195, Japan

<sup>2</sup>Condensed Matter and Magnet Science, Los Alamos National Laboratory, Los Alamos, New Mexico 87545, USA

<sup>3</sup>Theoretical Division, Los Alamos National Laboratory, Los Alamos, New Mexico 87545, USA

(Received 9 February 2015; published 10 September 2015)

Chemical substitutions are used commonly to tune a magnetic transition to zero temperature, but the resulting non-Fermi-liquid (NFL) behavior is nonuniversal. We have used nuclear quadrupole resonance to probe microscopically the response of a prototypical quantum critical metal CeCoIn<sub>5</sub> to substitutions of small amounts of Sn and Cd for In. These substituents induce very different local electronic environments as observed by site-dependent spin lattice relaxation rates  $1/T_1$  that influence the NFL behavior. The effects found here illustrate the need for care in interpreting NFL properties determined by macroscopic measurements.

DOI: [10.1103/PhysRevB.92.121105](https://doi.org/10.1103/PhysRevB.92.121105)

PACS number(s): 71.27.+a, 74.40.Kb, 76.60.-k

Quantum critical points (QCPs) are an excellent organizing principle for the non-Fermi-liquid (NFL) behavior observed in many systems and are a source of fluctuations from which unconventional superconductivity (SC) emerges. There are numerous examples in a wide range of different materials systems where chemical substitutions have been used to induce NFL states or to tune a magnetic transition to zero temperature [1–3]. These substitutions certainly induce disorder scattering but also may create an effective chemical pressure or, if non-isoelectronic, change the electron count and shift the chemical potential. Experimentally, quite often it is difficult to untangle which of these contribute dominantly to the NFL or quantum critical behaviors, and most theoretical models are nonspecific to a particular type of substitution. An interesting case where the role of substitutions might be tested explicitly would be to intentionally introduce a small number of substituents into a material that, in pure form, is at or very close to a QCP. The heavy-fermion compound CeCoIn<sub>5</sub> is one of the few materials in which this test might be made.

CeCoIn<sub>5</sub> is an unconventional superconductor that belongs to the CeTIn<sub>5</sub> ( $T = \text{Co, Rh, Ir}$ ) family, and is known to lie in close proximity to an AFM QCP at ambient pressure [4,5]. Due to the high purity of the parent materials we can study how controlled amounts of disorder influence these phenomena. Specifically, we consider disorder introduced by Cd or Sn substitutions for In. Besides producing disorder, these substituents also nominally hole- (Cd) or electron- (Sn) doped CeCoIn<sub>5</sub>. As summarized in Fig. 1, a small amount of Cd ( $5s^2$ ) substitution for In ( $5s^25p$ ) induces long-range AFM order [6]. For  $\sim 1\%$  Cd substitution the AFM propagation vector is  $\mathbf{Q} = (\frac{1}{2}, \frac{1}{2}, \frac{1}{2})$  and the ordered moment is  $\sim 0.7 \mu_B/\text{Ce}$  [7,8]. Applying pressure suppresses the AFM; however, the fluctuations and the signatures in electrical transport properties at this pressure ( $P$ ) induced AFM QCP are absent [9]. A recent study of Cd-doped CeIrIn<sub>5</sub> draws the same conclusions [10]. These observations are in contrast to the  $T$ - $P$  diagram of both pure and Sn-doped CeRhIn<sub>5</sub> for which the NFL signatures are still present at its pressure-induced AFM QCP [11,12]; i.e., random distributions of dilute Sn dopants do not destroy

signatures of quantum criticality. In the case of Sn ( $5s^25p^2$ ) substitution in CeCoIn<sub>5</sub>, magnetic order is not induced, and instead the AFM fluctuations are suppressed as the system is driven away from the AFM QCP [13,14]. This conclusion is not a consequence of an induced chemical pressure but rather is due to stronger  $f$ - $c$  hybridization induced by the Sn dopants [15]. Further, as shown in Fig. 1, the SC dome for  $\sim 1\%$  Cd substitution remains broad in the  $T$ - $P$  plane as in the pure CeCoIn<sub>5</sub> [16], but shrinks monotonically by Sn substitution [17]. This dichotomy in CeCoIn<sub>5</sub>'s response to Sn and Cd substitutions poses the essential question of why the two nonmagnetic dopants on the In sites could produce vastly different responses.

In this Rapid Communication, we report a qualitative difference in local electronic environments around Sn and Cd substituents that is probed by nuclear quadrupole resonance (NQR). As we show, Sn substitutions introduce a rather homogeneous electronic state suppressing the AFM fluctuations, but Cd substitutions produce an electronic heterogeneous state where Cd dopants enhance AFM behavior by inducing unscreened localized moments below Kondo energy scale  $T_K$  in their immediate vicinity. In effect, dilute Cd-doped CeCoIn<sub>5</sub> becomes an ideal *Kondo hole* system in a quantum critical metal.

Single crystals of CeCoIn<sub>5</sub>, CeCoIn<sub>4.85</sub>Sn<sub>0.15</sub> (termed 3% Sn-doped), and CeCoIn<sub>4.925</sub>Cd<sub>0.075</sub> (1.5% Cd-doped) were grown by the self-flux method [18,19]. Small crystals for zero-field NQR studies were selected from the same batch used for magnetic susceptibility, electrical resistivity, and specific-heat measurements. The AFM transition temperature  $T_N$  for the 1.5% Cd-doped sample is 3.7 K [20]. Microprobe measurement using wavelength-dispersive spectroscopy and the extended x-ray absorption fine structure (EXAFS) observe a homogeneous distribution of both Sn and Cd with a preferential occupation on the In(1) site [21,22].

As shown at the top of Fig. 1, CeCoIn<sub>5</sub> forms in the tetragonal HoCoGa<sub>5</sub>-type structure ( $P4/mmm$ ) with two crystallographically inequivalent In sites denoted as In(1) ( $4/mmm$ ) and In(2) ( $2mm$ ). The Ce sites are surrounded on all sides by 4 nearest-neighbor (nn) In(1) (at 3.26 Å) and 8 nn In(2) atoms (at 3.28 Å) [23]. Using the conventional definition of the electric field gradient (EFG), the NQR frequency  $\nu_Q$  is

\*sakai.hironori@jaea.go.jp

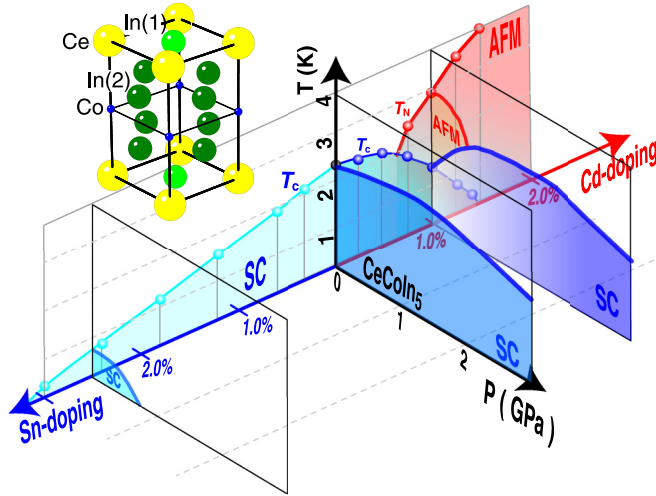


FIG. 1. (Color online) Phase diagram for Sn and Cd doped  $\text{CeCoIn}_5$  and the crystal structure of  $\text{CeCoIn}_5$ .  $T$ - $P$  diagrams are also drawn for  $\text{CeCoIn}_5$  [16], Sn-doped  $\text{CeCoIn}_5$  [17], and Cd-doped  $\text{CeCoIn}_5$  [9].

defined as  $3e^2qQ/\{2I(2I-1)h\}$  by the nuclear quadrupolar moment  $eQ$  and the principal component of the EFG tensor  $eq \equiv V_{ZZ}$ . For a nonaxial EFG, the asymmetry parameter is defined as  $\eta \equiv \{|V_{YY}| - |V_{XX}|\}/|V_{ZZ}|$  ( $|V_{XX}| \leq |V_{YY}| \leq |V_{ZZ}|$ ). The  $^{115}\text{In}$  NQR spectrum for  $\text{CeCoIn}_5$  consists of 4 lines for In(1) sites with an equal separation of  $\nu_Q = 8.17$  MHz and  $\eta = 0$ , and 4 unequally separated lines for In(2) sites whose positions give  $\nu_Q = 15.5$  MHz and  $\eta = 0.39$  [24], by diagonalization of the electric quadrupole Hamiltonian  $\mathcal{H}_Q = (h\nu_Q/6)\{3I_z^2 - I(I+1) + (\eta/2)(I_+^2 + I_-^2)\}$ .

In Sn- and Cd-substituted  $\text{CeCoIn}_5$ , as shown in Fig. 2(a), the  $4\nu_Q$  line for In(1) splits into a main peak (A) and several satellite peaks labeled B, C, and D. The split In(1) spectrum

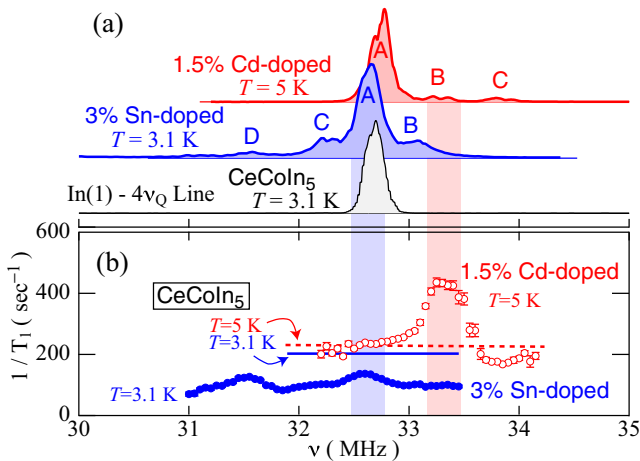


FIG. 2. (Color online) (a) In(1)- $4\nu_Q$  NQR spectra for  $\text{CeCoIn}_5$ , 3% Sn-doped, and 1.5% Cd-doped  $\text{CeCoIn}_5$  in the paramagnetic (normal) state. The upper case labels A, B, C, and D indicate the respective spectral positions. (b) Frequency dependence of  $1/T_1$  for the  $4\nu_Q$  line on In(1) sites in 3% Sn-doped and 1.5% Cd-doped  $\text{CeCoIn}_5$ , having a common frequency axis with the above NQR spectra. Values of  $1/T_1$  at the NQR peak of  $\text{CeCoIn}_5$  at 3.1 K and 5 K are represented by solid and dashed line, respectively.

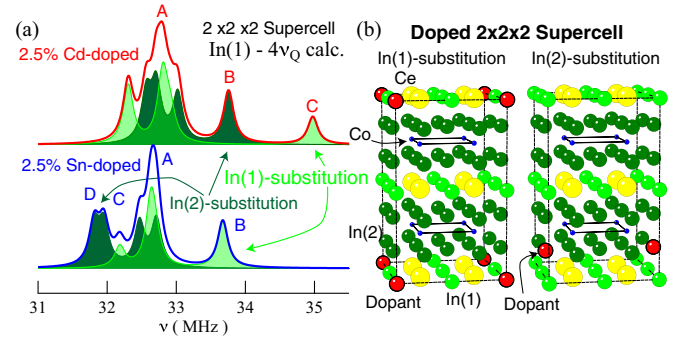


FIG. 3. (Color online) (a) Calculated spectral shape for  $4\nu_Q$  of In(1) NQR and  $3\nu_Q$  of In(2) NQR. The light and dark (green) shades originate from dopants on the In(1) and In(2) sites, respectively. (b) The assumed  $2 \times 2 \times 2$  supercell.

for the Cd case is consistent with previous reports [8]. The resolved line splittings mean that the local EFGs for the A, B, C, and D peaks are discretely distributed for sites near the Sn or Cd. Similar splittings are observed for the other transition lines at  $\nu_Q$ ,  $2\nu_Q$ , and  $3\nu_Q$ , although the A, B, C, and D peaks partly overlap. The EFGs even for the main peak A, which corresponds to bulk In(1) sites well separated from the Sn or Cd, have finite  $\eta$ ; i.e., the tetragonal symmetry is locally broken. We estimate  $\eta$  for A, B, and C sites for Sn (Cd) substitutions to be 0.025 (0.005), 0.02 (0.09), and 0.02 (0.12), respectively. For Cd substitution,  $\eta$  for the bulk A line is much smaller than in the Sn case. The EFG may be decomposed into intra-atomic and inter-atomic contributions. Since the former would not be site specific, the latter must be the main source of an EFG distortion of the bulk sites. In contrast, there is no clear splitting for the In(2) sites [20], and the lines just broaden in the Sn case and become more complicated in the Cd case, which may be due to a nondiscrete distribution of EFGs induced on the In(2) sites by substitution.

For spectral assignment, EFGs have been calculated by density functional theory (DFT) [14,20] assuming 2.5% Sn (Cd) doping in a  $2 \times 2 \times 2$  supercell in Fig. 3. The DFT calculations were performed using the WIEN2K code [25] with the exchange correlation potentials [26]. Calculated spectra for substitutions on the In(1) and In(2) sites are summed because the fractional occupancy for the dopant atoms on these sites is roughly 50/50 for both Cd and Sn doping [21,22]. For each doped supercell, the NQR lines are calculated by solving  $\mathcal{H}_Q$ , with the assumption of a natural width of 100 kHz for the calculated EFG on every In site, and then they are summed. To compare with experimental results, the computed spectral frequencies are multiplied by a factor of  $\sim 0.9$ , which may be attributed to screening of EFGs by conduction electrons in the real lattice. A similar approach has been reported earlier [27]. In both doped cases, these calculations reproduce the main NQR spectral features; e.g., the In(1) NQR lines are rather discrete compared to the In(2) lines. From a comparison with the calculations, we assign the B line to the In(1) nn sites for Sn substitutions. In the Cd-doped sample, B and C lines are attributed to the nn In(1) sites for Cd substituted on In(2) and In(1) sites, respectively.

Our primary findings are the respective peak dependencies of the nuclear spin-lattice relaxation rates  $1/T_1$  for the In(1)

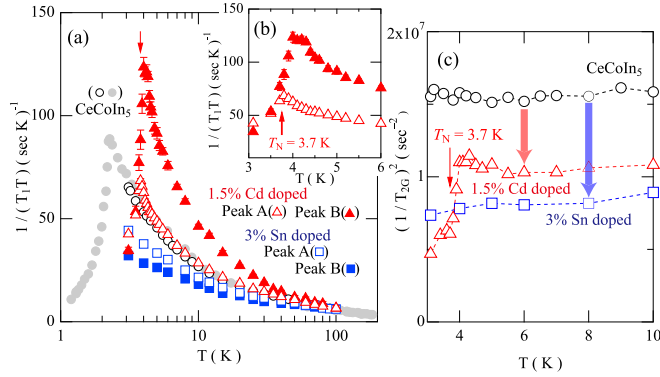


FIG. 4. (Color online) (a) Temperature dependence of the longitudinal relaxation rate divided by temperature  $1/T_1T$ . (b) Magnified  $(T_1T)^{-1}-T$  plot in the low-temperature range. (c) Square of the Gaussian transverse relaxation rate  $1/T_{2G}^2$ . Data are shown for In(1) NQR in CeCoIn<sub>5</sub>, 3% Sn-doped, and 1.5% Cd-doped CeCoIn<sub>5</sub>, which were measured at the main A peak for doped CeCoIn<sub>5</sub>. The  $1/T_1T$  data for CeCoIn<sub>5</sub> are also plotted for a wide temperature range from Ref. [29].

sites, which are shown Fig. 2(b) [20]. In the case of finite  $\eta$ , the recovery function was calculated by numerical diagonalization of the master equation for nuclear relaxation [28]. For the Sn substitutions,  $1/T_1$  is reduced on average, and the variation in the magnitude of  $1/T_1$  is small.  $1/T_1$  values for the bulk A and satellite D peaks show a maximum, while those for B and C peaks are diminished. In contrast, with Cd doping,  $1/T_1$  is most prominent at peak B, not at the bulk A peak in  $4\nu_Q$  nor at peak C; i.e., the AFM spin fluctuations are enhanced only at the In(1) sites that are nn to Cd substituted In(2) sites.

The  $T$  dependence of  $1/T_1T \propto \sum_q \text{Im}\chi_{\perp}(\mathbf{q}, \omega_0)/\omega_0$  for A and B peaks in doped CeCoIn<sub>5</sub> is shown in Fig. 4(a). In this expression  $\chi(\mathbf{q}, \omega)$  is the dynamical susceptibility. At temperatures above 100 K, all  $1/T_1T$  data appear to merge with data for undoped CeCoIn<sub>5</sub>. This reflects a homogeneous electronic state in both doped cases at high temperatures, where the  $4f$  spin fluctuations behave as if localized so that  $1/T_1$  becomes constant above  $T^*$ . The crossover temperature  $T^*$  between localized and itinerant regimes is  $\sim 150$  K in CeCoIn<sub>5</sub> [29]. As reported earlier [30], well below  $T^*$ ,  $1/T_1$  shows a characteristic  $T^{1/4}$  dependence above  $T_c = 2.3$  K due to anisotropic AFM spin fluctuations associated with proximity to an AFM QCP. In addition, the field dependence of  $1/T_1T$  in CeCoIn<sub>5</sub> is well understood quantitatively by the self-consistent renormalization (SCR) theory for an itinerant SDW model of criticality [5]. Below  $T^*$ ,  $1/T_1T$  for A and B peaks in the Sn-doped case deviates downward from those for undoped CeCoIn<sub>5</sub>, indicating a rather uniform reduction of electronic correlations. With Cd substitution, the  $T$  dependence of  $1/T_1T$  for the bulk A sites above  $T_N = 3.7$  K is the same as in CeCoIn<sub>5</sub>. That is, the majority of the Cd-doped sample is in the same electronic state as in undoped CeCoIn<sub>5</sub>. On the other hand,  $1/T_1T$  for the B sites is significantly enhanced and  $1/T_1$  is nearly  $T$ -independent; i.e., a small group of sites neighboring Cd ions that reside on In(2) sites remains unscreened by conduction electrons. In addition, a maximum in  $(T_1T)^{-1}$  for the B peak occurs slightly higher than  $T_N$ , as

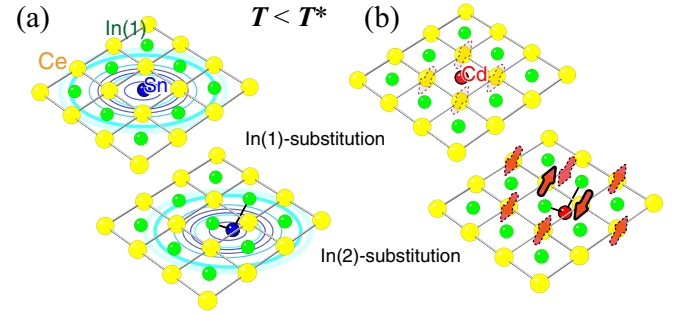


FIG. 5. (Color online) Schematic illustrations for the microscopic circumstances around (a) Sn and (b) Cd dopants.

shown in Fig. 4(b), which suggests that short-range AFM order develops around the B sites above the bulk  $T_N$ .

The nuclear spin-spin relaxation rate  $1/T_2$  provides a measure of the magnetic correlation length  $\xi$ . As in pure CeCoIn<sub>5</sub>, the echo decay  $E(2\tau)$  can be fitted to  $E(2\tau) = E(0) \exp(-2\tau/T_{2L}) \exp[-\frac{1}{2}(2\tau/T_{2G})^2]$  with  $\tau$  being the separation time between excitation and refocusing pulses. In a strongly correlated metal,  $1/T_2$  contains the  $T_1$  process which is represented by Lorentz-type decay on a scale  $T_{2L}$  and an indirect (nuclear) spin-spin coupling by Gaussian-type decay with a time scale  $T_{2G}$ . Since the  $T$  dependence and orders of magnitude of the obtained  $1/T_{2L}$  are consistent with the converted  $1/T_1$  values from NQR [20,31,32], our estimates of  $1/T_{2G}$  are reasonable. An oscillation of the echo decay is observed only for the B peak with Sn doping; i.e.,  $E(2\tau)$  has an additional term of the form  $\cos(J\tau)$  with  $J \sim 1.5$  kHz [20], which may come from pseudo-dipolar type interactions via additional  $5p$  electrons on the Sn atoms with long-range coherence ( $\propto 1/r_i^3$ ), although such an echo decay oscillation is widely observed in systems having nuclear quadrupolar interactions [33] or in dilute nuclear spin systems [34].

As shown in Fig. 4(c),  $1/T_{2G}^2 \propto \int \text{Re}\chi^2(\mathbf{q}, 0) d\mathbf{q}$  [35,36] is nearly  $T$ -independent below  $\sim 6$  K except for a decrease just above  $T_N$  in Cd-doped CeCoIn<sub>5</sub>. In the paramagnetic state for a strongly correlated system, the static scaling law  $\text{Re}\chi(\mathbf{q}, 0) \sim \xi^2 g(q\xi, 0)$  holds with a scaling function  $g$  such that  $(1/T_{2G}^2) \sim \xi(T)$  [37].  $\xi(T \rightarrow 0)/a$  for pure CeCoIn<sub>5</sub> has been already estimated to be about 2 at the low temperature [5,38]. The bulk  $T$ -independent values in Sn- and Cd-doped crystals are reduced roughly by a factor of 1/2 to 2/3 relative to pure CeCoIn<sub>5</sub>, as displayed by the thick arrows in Fig. 4(c). Therefore, we deduce that both Cd and Sn doping reduce  $\xi/a$  to approximately unity.

We summarize our results schematically in Fig. 5. Sn substitution for both In(1) and In(2) acts to locally enhance  $p-f$  hybridization with long-range spatial coherence. Thus, the  $4f$  electronic state is uniformly pushed to the more itinerant side of the AFM-QCP. The diffuse potential around Sn dopants also acts as a nonmagnetic scattering center thereby suppressing  $T_c$  of this unconventional superconductor. In contrast, Cd dopants on In(2) sites enhance the magnetization in their vicinity, inducing localized spins on neighboring Ce sites, while the majority of the electronic states remain unchanged. The nucleation of short-range ordering near the Cd dopants (developing around 4.1 K) triggers long-range AFM ordering

throughout the sample, observed as a bulk transition at 3.7 K. Interestingly, Cd dopants on In(1) sites do not induce local moments, proving anisotropic  $p$ - $f$  hybridization paths between Ce-In(1) and Ce-In(2) [39]. With applied pressure, the induced local moments around Cd dopants can be screened again, and AFM ordering is suppressed. Consequently, the SC dome in  $T$ - $P$  is nearly identical to that for CeCoIn<sub>5</sub>. Such a heterogeneous electronic state has been thoroughly explored by NMR studies of cuprate and Fe-based superconductors [40,41].

What is the origin of the difference between Cd and Sn doping? DFT calculations capture the fact that hybridization on average increases for Sn doping and decreases with Cd doping [14]. Due to potential stability of the full  $d$  shell,  $p$  holes on Cd dopants are ineffective in promoting hybridization between Ce and In(2) sites and consequently contribute little to the bulk electronic bands, but the additional  $p$  electrons in Sn dopants enhance the  $p$ - $f$  hybridizations. We note that comparable behavior can be inferred from doping studies on an antiferromagnet CeIn<sub>3</sub>. Cd doping in CeIn<sub>3</sub> has primarily a local effect and an AFM QCP has not been reached [42], but Sn doping leads to a strongly hybridized state, with clear signatures of NFL behavior at the QCP and eventually a mixed valent state in CeSn<sub>3</sub> [43].

The role of nonmagnetic defects has been studied within the Kondo lattice model [44]. In this model, AFM correlations are enhanced and locally bound  $f$  states with spatial scale

$\xi/a_0 \sim 0.65$  in an ideal square lattice are predicted to appear in the vicinity of Kondo holes, which are voids in the heavy-fermion liquid state. This heterogeneous electronic state is closely analogous to that in Cd-doped CeCoIn<sub>5</sub>. To understand nonuniversal NFL behaviors [2] in a unified way, dynamics of Kondo holes in a quantum critical system should be further investigated, since heterogeneous electronic states appear to be realized in a variety of correlated electron systems. For instance, it is interesting to ask what is the degree and influence of electronic heterogeneity in YbRh<sub>2</sub>Si<sub>2</sub>, particularly, given the nearly field-independent local to itinerant crossover in pressure-tuned and Co- and Ir-doped YbRh<sub>2</sub>Si<sub>2</sub> [45,46]. Moreover, a dynamical electronic heterogeneity at a QCP accessed by an applied magnetic field was also revealed by NMR studies even in pure YbRh<sub>2</sub>Si<sub>2</sub> [47]. Electronic heterogeneity may also hold for Rh-doped CeCoIn<sub>5</sub> [48]. These observations are important for unifying the nonuniversal NFL and quantum critical behavior observed in many systems.

We thank Y. Haga for supplying single crystals of CeCoIn<sub>5</sub>. We also thank T. Hattori, H. Ikeda, R. R. Urbano, Z. Fisk, and R. E. Walstedt for valuable discussions. Work in Japan was supported by the Reimei Research Program of JAEA. Work at LANL was performed under the auspices of the US DOE, Office of Basic Energy Sciences, Division of Materials Sciences and Engineering.

- 
- [1] H. v. Löhneysen, A. Rosch, M. Vojta, and P. Wölfle, *Rev. Mod. Phys.* **79**, 1015 (2007).
- [2] G. R. Stewart, *Rev. Mod. Phys.* **73**, 797 (2001).
- [3] E. Miranda and V. Dobrosavljević, *Rep. Prog. Phys.* **68**, 2337 (2005).
- [4] C. Petrovic, P. G. Pagliuso, M. F. Hundley, R. Movshovich, J. L. Sarrao, J. D. Thompson, Z. Fisk, and P. Monthoux, *J. Phys.: Condens. Matter* **13**, L337 (2001).
- [5] H. Sakai, S. E. Brown, S. H. Baek, F. Ronning, E. D. Bauer, and J. D. Thompson, *Phys. Rev. Lett.* **107**, 137001 (2011).
- [6] L. D. Pham, T. Park, S. Maquilon, J. D. Thompson, and Z. Fisk, *Phys. Rev. Lett.* **97**, 056404 (2006).
- [7] M. Nicklas, O. Stockert, T. Park, K. Habicht, K. Kiefer, L. D. Pham, J. D. Thompson, Z. Fisk, and F. Steglich, *Phys. Rev. B* **76**, 052401 (2007).
- [8] R. R. Urbano, B. L. Young, N. J. Curro, J. D. Thompson, L. D. Pham, and Z. Fisk, *Phys. Rev. Lett.* **99**, 146402 (2007).
- [9] S. Seo, X. Lu, J.-X. Zhu, R. R. Urbano, N. Curro, E. D. Bauer, V. A. Sidorov, L. D. Pham, T. Park, Z. Fisk, and J. D. Thompson, *Nat. Phys.* **10**, 120 (2014).
- [10] Y. Chen, W. B. Jiang, C. Y. Guo, F. Ronning, E. D. Bauer, T. Park, H. Q. Yuan, Z. Fisk, J. D. Thompson, and X. Lu, *Phys. Rev. Lett.* **114**, 146403 (2015).
- [11] S. Seo, E. Park, E. D. Bauer, F. Ronning, J. N. Kim, J. H. Shim, J. D. Thompson, and T. Park, *Nat. Commun.* **6**, 6433 (2015).
- [12] T. Park, F. Ronning, H. Q. Yuan, M. B. Salamon, R. Movshovich, J. L. Sarrao, and J. D. Thompson, *Nature (London)* **440**, 65 (2006).
- [13] E. D. Bauer, F. Ronning, C. Capan, M. J. Graf, D. Vandervelde, H. Q. Yuan, M. B. Salamon, D. J. Mixson, N. O. Moreno, S. R. Brown, J. D. Thompson, R. Movshovich, M. F. Hundley, J. L. Sarrao, P. G. Pagliuso, and S. M. Kauzlarich, *Phys. Rev. B* **73**, 245109 (2006).
- [14] K. Gofryk, F. Ronning, J. X. Zhu, M. N. Ou, P. H. Tobash, S. S. Stoyko, X. Lu, A. Mar, T. Park, E. D. Bauer, J. D. Thompson, and Z. Fisk, *Phys. Rev. Lett.* **109**, 186402 (2012).
- [15] E. D. Bauer, N. O. Moreno, D. J. Mixson, J. L. Sarrao, J. D. Thompson, M. F. Hundley, R. Movshovich, and P. G. Pagliuso, *Physica B* **359–361**, 35 (2005).
- [16] V. A. Sidorov, M. Nicklas, P. G. Pagliuso, J. L. Sarrao, Y. Bang, A. V. Balatsky, and J. D. Thompson, *Phys. Rev. Lett.* **89**, 157004 (2002).
- [17] S. M. Ramos, M. B. Fontes, E. N. Hering, M. A. Continentino, E. Baggio-Saitovich, F. D. Neto, E. M. Bittar, P. G. Pagliuso, E. D. Bauer, J. L. Sarrao, and J. D. Thompson, *Phys. Rev. Lett.* **105**, 126401 (2010).
- [18] E. D. Bauer, C. Capan, F. Ronning, R. Movshovich, J. D. Thompson, and J. L. Sarrao, *Phys. Rev. Lett.* **94**, 047001 (2005).
- [19] Y. Tokiwa, R. Movshovich, F. Ronning, E. D. Bauer, P. Papin, A. D. Bianchi, J. F. Rauscher, S. M. Kauzlarich, and Z. Fisk, *Phys. Rev. Lett.* **101**, 037001 (2008).
- [20] See Supplemental Material at <http://link.aps.org/supplemental/10.1103/PhysRevB.92.121105> for (i) the bulk  $T_N$  determination in 1.5% Cd-doped sample, (ii) the NQR spectrum for In(2) sites and comparison with DFT calculations, (iii) frequency

- dependence of  $1/T_1$ , and (iv) the echo decay curves for  $T_2$  measurements.
- [21] M. Daniel, E. D. Bauer, S. W. Han, C. H. Booth, A. L. Cornelius, P. G. Pagliuso, and J. L. Sarrao, *Phys. Rev. Lett.* **95**, 016406 (2005).
- [22] C. H. Booth, E. D. Bauer, A. D. Bianchi, F. Ronning, J. D. Thompson, J. L. Sarrao, J. Y. Cho, J. Y. Chan, C. Capan, and Z. Fisk, *Phys. Rev. B* **79**, 144519 (2009).
- [23] E. G. Moshopoulou, J. L. Sarrao, P. G. Pagliuso, N. O. Moreno, J. D. Thompson, Z. Fisk, and R. M. Ibberson, *Appl. Phys. A (Suppl.)* **74**, 895 (2002).
- [24] Y. Kohori, Y. Yamato, Y. Iwamoto, T. Kohara, E. D. Bauer, M. B. Maple, and J. L. Sarrao, *Phys. Rev. B* **64**, 134526 (2001).
- [25] P. Blaha, K. Schwarz, G. Madsen, D. Kvasnicka, and J. Luitz, WIEN2K, *An Augmented Plane Wave + Local Orbitals Program for Calculating Crystal Properties* (K. Schwarz, Tech. Universität Wien, Austria, 2001).
- [26] J. P. Perdew, K. Burke, and M. Ernzerhof, *Phys. Rev. Lett.* **77**, 3865 (1996).
- [27] J. Ruzs, P. M. Oppeneer, N. J. Curro, R. R. Urbano, B.-L. Young, S. Lebègue, P. G. Pagliuso, L. D. Pham, E. D. Bauer, J. L. Sarrao, and Z. Fisk, *Phys. Rev. B* **77**, 245124 (2008).
- [28] J. Chepin and J. J. H. Ross, *J. Phys.: Condens. Matter* **3**, 8103 (1991).
- [29] M. Yashima, S. Kawasaki, Y. Kawasaki, G.-q. Zheng, Y. Kitaoka, H. Shishido, R. Settai, Y. Haga, and Y. Ōnuki, *J. Phys. Soc. Jpn.* **73**, 2073 (2004).
- [30] Y. Kawasaki, S. Kawasaki, M. Yashima, T. Mito, G.-q. Zheng, Y. Kitaoka, H. Shishido, R. Settai, Y. Haga, and Y. Ōnuki, *J. Phys. Soc. Jpn.* **72**, 2308 (2003).
- [31] N. J. Curro and D. Pines, *J. Phys. Chem. Solids* **68**, 2028 (2007).
- [32] R. E. Walstedt, *Phys. Rev. Lett.* **19**, 146 (1967); **19**, 816(E) (1967).
- [33] H. Abe, H. Yasuoka, M. Matsuura, A. Hirai, and T. Shinjo, *J. Phys. Soc. Jpn.* **19**, 1491 (1964).
- [34] C. Froidevaux and M. Weger, *Phys. Rev. Lett.* **12**, 123 (1964).
- [35] C. H. Pennington and C. P. Slichter, *Phys. Rev. Lett.* **66**, 381 (1991).
- [36] R. E. Walstedt and S.-W. Cheong, *Phys. Rev. B* **51**, 3163 (1995).
- [37] S. Kambe, H. Sakai, Y. Tokunaga, T. D. Matsuda, Y. Haga, H. Chudo, and R. E. Walstedt, *Phys. Rev. Lett.* **102**, 037208 (2009).
- [38] C. Stock, C. Broholm, J. Hudis, H. J. Kang, and C. Petrovic, *Phys. Rev. Lett.* **100**, 087001 (2008).
- [39] K. Haule, C.-H. Yee, and K. Kim, *Phys. Rev. B* **81**, 195107 (2010).
- [40] P. M. Singer, A. W. Hunt, and T. Imai, *Phys. Rev. Lett.* **88**, 047602 (2002).
- [41] F. Ning, K. Ahilan, T. Imai, A. S. Sefat, R. Jin, M. A. McGuire, B. C. Sales, and D. Mandrus, *J. Phys. Soc. Jpn.* **78**, 013711 (2009).
- [42] N. Berry, E. M. Bittar, C. Capan, P. G. Pagliuso, and Z. Fisk, *Phys. Rev. B* **81**, 174413 (2010).
- [43] P. Pedrazzini, M. G. Berisso, N. Caroca-Canales, M. Deppe, C. Geibel, and J. G. Sereni, *Eur. Phys. J. B* **38**, 445 (2004).
- [44] J. Figgins and D. K. Morr, *Phys. Rev. Lett.* **107**, 066401 (2011).
- [45] Y. Tokiwa, P. Gegenwart, C. Geibel, and F. Steglich, *J. Phys. Soc. Jpn.* **78**, 123708 (2009).
- [46] S. Friedemann, T. Westerkamp, M. Brando, N. Oeschler, S. Wirth, P. Gegenwart, C. Krellner, C. Geibel, and F. Steglich, *Nat. Phys.* **5**, 465 (2009).
- [47] S. Kambe, H. Sakai, Y. Tokunaga, G. Lapertot, T. D. Matsuda, G. Knebel, J. Flouquet, and R. E. Walstedt, *Nat. Phys.* **10**, 840 (2014).
- [48] S. K. Goh, J. Paglione, M. Sutherland, E. C. T. O'Farrell, C. Bergemann, T. A. Sayles, and M. B. Maple, *Phys. Rev. Lett.* **101**, 056402 (2008).